ARTICLES
https://doi.org/10.1038/s41593-019-0394-3
nature neuroscience

Compulsivity and impulsivity traits linked to attenuated developmental frontostriatal myelination trajectories

Gabriel Ziegler[1,2,3,4,12*], Tobias U. Hauser[1,2,12*], Michael Moutoussis[1,2], Edward T. Bullmore[5,6,7,8], Ian M. Goodyer[5,6], Peter Fonagy[9], Peter B. Jones[5,6], NSPN Consortium[10], Ulman Lindenberger[1,11] and Raymond J. Dolan[1,2]

The transition from adolescence to adulthood is a period when ongoing brain development coincides with a substantially increased risk of psychiatric disorders. The developmental brain changes accounting for this emergent psychiatric symptomatology remain obscure. Capitalizing on a unique longitudinal dataset that includes in vivo myelin-sensitive magnetization transfer (MT) MRI scans, we show that this developmental period is characterized by brain-wide growth in MT trajectories within both gray matter and adjacent juxtacortical white matter. In this healthy population, the expression of common developmental traits, namely compulsivity and impulsivity, is tied to a reduced growth of these MT trajectories in frontostriatal regions. This reduction is most marked in dorsomedial and dorsolateral prefrontal regions for compulsivity and in lateral and medial prefrontal regions for impulsivity. These findings highlight that psychiatric traits of compulsivity and impulsivity are linked to regionally specific reductions in myelin-related growth in late adolescent brain development.

Structural brain development extends into adulthood, particularly in regions that mediate higher cognition such as the prefrontal cortex[1]. A canonical view is that this maturation is characterized by regional shrinkage in gray matter (GM) coupled to an expansion of white matter (WM)[2]. However, the underlying microstructural processes remain obscure. Two candidate mechanisms have been proposed[3], namely, (1) synaptic loss (pruning) that reduces supernumerary connections and (2) an increase in myelination that serves to enhance communication efficiency. Both accounts receive a degree of support from cross-sectional and ex vivo studies[4–7]. What is also known is that there are substantial inter-individual differences in these growth trajectories[8], with the most marked changes occurring within an age window in which an emergence of psychiatric illness is increasingly common[9,10]. This raises the possibility that this enhanced psychiatric risk is tied to altered maturational brain trajectories during this critical developmental period[11,12].

Compulsivity and impulsivity are two important symptom dimensions in psychiatry[13] that also show substantial variation in expression within a healthy population (Supplementary Fig. 1a–f). At the extreme, compulsivity and impulsivity can manifest as obsessive–compulsive disorder (OCD) and attention-deficit/hyperactivity disorder, respectively. Macrostructural and cross-sectional studies have suggested a link to changes in frontostriatal regions[13–16]. However, the question of whether compulsivity and impulsivity reflect consequences of altered developmental microstructural processes remains unanswered.

Here, we used semiquantitative structural MRI[17] to investigate microstructural brain development during the transition to adulthood, specifically seeking whether individual variability in these developmental brain trajectories is linked to the expression of compulsive and impulsive traits. We used a novel MT imaging protocol to provide an in vivo marker for macromolecules, in particular myelin[18,19]. Importantly, MT saturation has been shown to be a more direct reflection of myelin compared with other imaging protocols, such as MT ratio[20,21]. It is also sensitive to developmental effects[7]. This renders it ideal for tracking patterns of brain maturation in longitudinal studies involving repeated scanning of participants, a crucial necessity for a full characterization of development[22]. Using such a protocol, we show that during late adolescence and early adulthood, the cingulate cortex expresses the greatest myelin-related growth, both within GM and adjacent WM. Individual differences in compulsivity were reflected in a reduced rate of this growth, particularly within dorsomedial and dorsolateral frontal regions. This contrasted with impulsivity, which was associated with reduced myelin-related growth in the lateral and medial prefrontal cortex. Our results suggest that within a healthy population, heterogeneity in compulsivity and impulsivity traits reflect regionally distinct differential growth in myelin growth trajectories.

Results

Ongoing myelin-related growth at the edge of adulthood. To assess developmental trajectories of myelin-sensitive MT scans, we exploited an accelerated longitudinal design that included

[1]Max Planck University College London Centre for Computational Psychiatry and Ageing Research, London, UK. [2]Wellcome Centre for Human Neuroimaging, University College London, London, UK. [3]Institute of Cognitive Neurology and Dementia Research, Otto-von-Guericke-University Magdeburg, Magdeburg, Germany. [4]German Center for Neurodegenerative Diseases (DZNE), Magdeburg, Germany. [5]Department of Psychiatry, University of Cambridge, Cambridge, UK. [6]Cambridgeshire and Peterborough National Health Service Foundation Trust, Cambridge, UK. [7]Medical Research Council/Wellcome Trust Behavioural and Clinical Neuroscience Institute, University of Cambridge, Cambridge, UK. [8]ImmunoPsychiatry, GlaxoSmithKline Research and Development, Stevenage, UK. [9]Research Department of Clinical, Educational and Health Psychology, University College London, London, UK. [10]A list of members appears in the Supplementary Note. [11]Center for Lifespan Psychology, Max Planck Institute for Human Development, Berlin, Germany. [12]These authors contributed equally: Gabriel Ziegler, Tobias U. Hauser. *e-mail: gabriel.ziegler@dzne.de; t.hauser@ucl.ac.uk

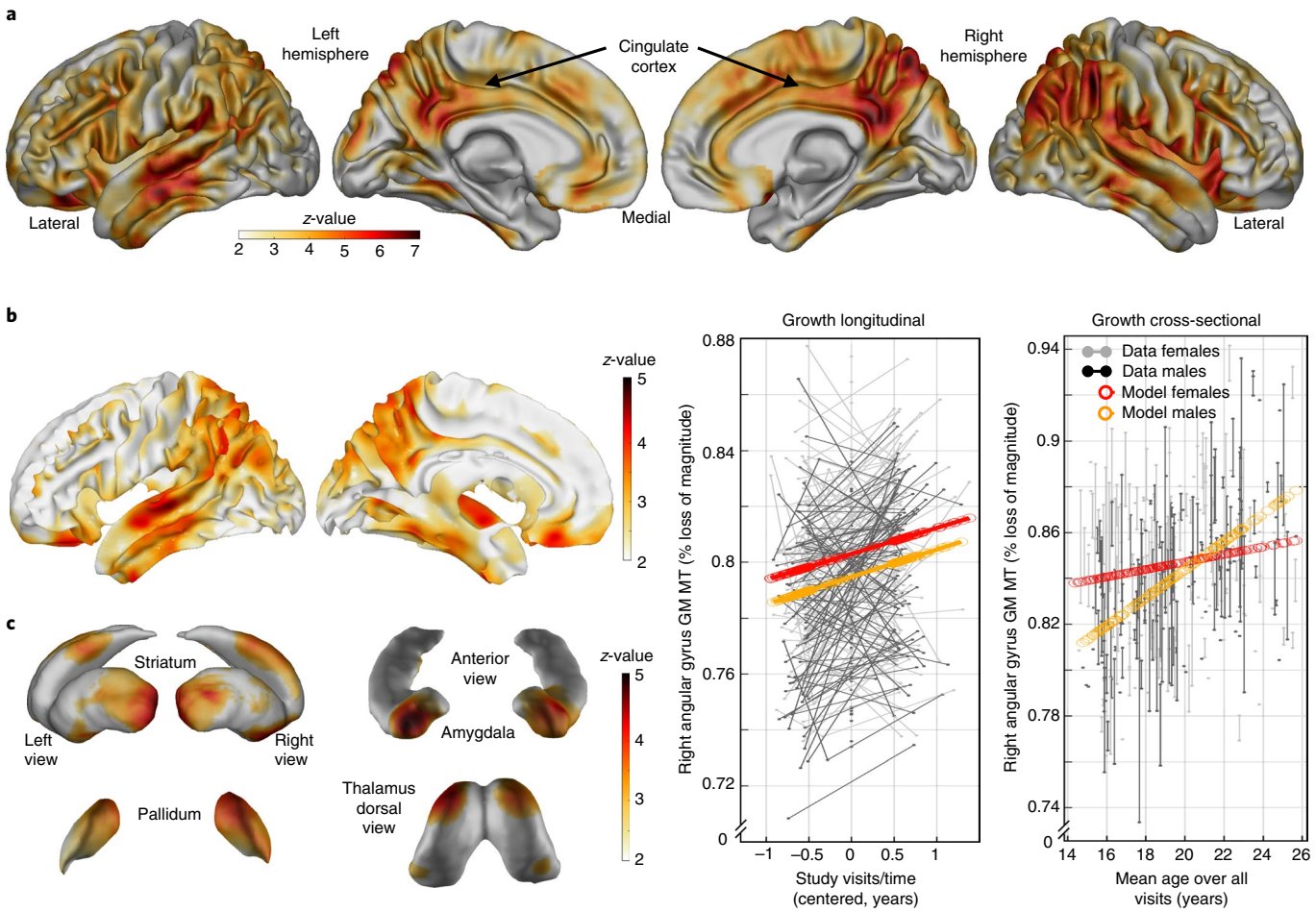

Fig. 1 | Developmental growth of myelin-sensitive MT into early adulthood. a–c, Transitioning into adulthood is characterized by marked increases in a myelin marker within cortical GM (**a**), adjacent cortical WM (**b**) and subcortical GM (**c**). Statistical *z*-maps of voxel-wise MT saturation show increases with time/visit (longitudinal) and age (cross-sectional). For specific effects of covariates (for example, time/visit, age, sex, interactions), see Supplementary Information. $n = 497/288$ scans/subjects, 51.7% female. **a**, MT increases in GM are strongest in the parietal, lateral temporal, posterior and middle cingulate, but are also present in prefrontal cortex. The projections illustrate statistical *z*-maps (colorbar indicates lower to higher *z* values with pale/yellow to dark/red shading) resulting from one-sided Wald tests ($P < 0.05$ FDR-corrected; sampling-based correction reported in Supplementary Table 1, and see also Supplementary Fig. 2c). The left plot shows the longitudinal model of right angular gyrus peak effects (mean across a 6-mm sphere; red and orange circles; see the right panel for definitions of colors), and adjusted data (gray/black) show MT growth in both sexes, with a marked sex difference reflecting greater MT in females (see Supplementary Fig. 3c for region-specific sex differences). The right plot shows corresponding cross-sectional model predictions in the same region, which exhibit a similar increase with age. *Y* axis refers to magnetization transfer saturation (% loss of magnetization). **b**, MT increase in adjacent cortical WM is most pronounced in the cingulate and parietotemporal cortex, with a coarse topographical correspondence to the MT effects in the GM. **c**, Subcortical GM nuclei express MT age-related effects in the striatum, pallidum, thalamus, amygdala and hippocampus (see also Fig. 2a,b). This growth pattern is most pronounced in the amygdala, ventral (maximum $z = 4.81$, $P = 0.004$ FDR; MNI: 20, 13, -11) and posterior ($z = 4.47$, $P = 0.004$ FDR; MNI: −31, −19, 3) striatum, suggesting ongoing myelin-associated changes in both cortical and subcortical brain structures.

repeated scanning of 288 (149 female) adolescents and young adults aged 14–24 years. The average follow-up time was 1.3 ± 0.32 years (mean ± s.d.) and up to three scans were performed (1 scan, $n = 100$; 2 scans, $n = 167$; 3 scans, $n = 21$). The sample was gender balanced and comprised otherwise healthy subjects (excluding self-reported illness a priori to avoid illness-related confounding factors, such as medication effects) who were selected to be approximately representative of the population (see Methods for details).

Examining individual, ongoing maturation using whole-brain voxel-based quantification analyses (Supplementary Fig. 2a,b) in GM revealed a brain-wide increase in myelin-related MT, with a strong emphasis within the cingulate, prefrontal and temporoparietal areas (Fig. 1a; $P < 0.05$ false-discovery rate (FDR) peak-corrected; merging cross-sectional and longitudinal effects). Overall mean change in GM voxels showing significant developmental effects (mean ± s.d.) was $0.58 \pm 0.19\%$ per year, with the strongest effect in the right angular gyrus ($z = 6.78$, $P < 0.002$ FDR) (Montreal Neurological Institute (MNI) coordinates: 51, −46, 44; 0.98% per year; see Supplementary Table 1 for parametric and nonparametric results, with separate cross-sectional and longitudinal effects shown in Supplementary Fig. 3a,b). These developmental changes were accompanied by increasing MT in adjacent (juxtacortical) superficial WM, with a topography similar to that seen in GM (Fig. 1b). The mean change in WM was $0.47 \pm 0.18\%$ per year, with the strongest effect in the posterior cingulate ($z = 6.18$, $P < 0.004$ FDR) (5, −58, 56; 0.89% per year; Supplementary Table 1). These results are consistent with the idea that connections within GM and WM are myelinated in concert (correlation between neighboring GM/WM voxels: Pearson $r = 0.25$, permutation $P < 0.001$; see also Methods). Similarly, albeit less pronounced, microstructural maturation was

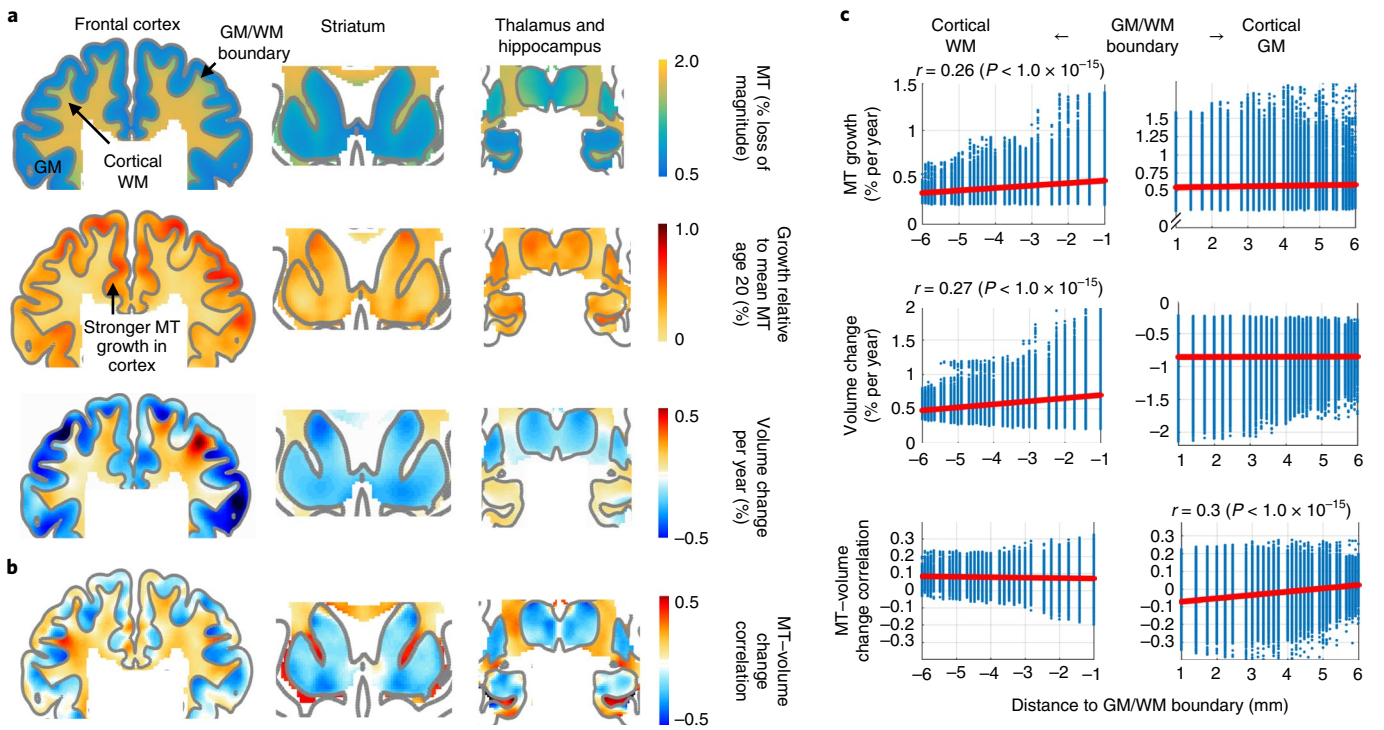

Fig. 2 | The relation between macrostructural and microstructural brain development. a, Coronal sections through the prefrontal cortex, striatal, and thalamus and hippocampus (MNI: $y = 15, 12, -14$) show more myelin-related MT in WM than in GM, with a clearly preserved GM/WM boundary (upper row, model intercept/mean, $n = 497/288$ scans/subjects, 51.7% female; sample details also apply to **b**). Beta parameters are shown to illustrate the sample mean level of MT (top row; mean age is about 20 years, accounting for covariates such as age, sex and confounds) and effect sizes of local changes of MT (middle row; relative to mean MT) and of changes of volume (bottom row); for statistical tests see Fig. 1 and Supplementary Fig. 4. Developmental changes in MT (middle row; averaged beta parameter of age and time/visit effects) illustrating the rate of change of our myelin marker in both tissue classes, with faster increases in GM areas. Developmental changes in macrostructural brain volume (bottom row; averaged beta parameter of age and time/visit effects) show a characteristic cortical shrinkage (blue) in GM, but an expansion in core and frontal WM (red; see also Supplementary Fig. 4). Only hippocampal GM shows an opposite effect, with continuing volume growth up to the verge of adulthood. **b**, Association between microstructural myelin growth and macrostructural volume change. A positive association throughout whole-brain WM supports the notion that myelination contributes to WM expansion. In GM, a predominantly negative association in deep layers points to partial volume effects at the tissue boundary (correlation was obtained from posterior covariance of beta parameters via SwE modeling, which simultaneously included longitudinal observations of both imaging modalities, unthresholded). **c**, Association as a function of Euclidean distance to the GM/WM boundary. Both tissue classes show consistent increases of MT (upper row; red line indicates linear regression; Pearson's correlation with distance and two-sided P values from corresponding t-distribution based on $n = 33{,}6164/11{,}8502$ voxels in cortical GM/WM), but opposite macrostructural volume change (middle row). Association between microstructural and macrostructural growth is positive in WM, independent of distance to the GM/WM boundary. In GM, the mean association changes from negative in deep layers (that is, myelin MT change associated with reduced GM volume) to slightly more positive associations in superficial layers (that is, MT associated with a tendency for increased GM volume).

observed in subcortical GM nuclei, including the amygdala, ventral and posterior striatum, pallidum and dorsal thalamus (Fig. 1c). The mean change in subcortical GM was $0.29 \pm 0.06\%$ per year, with strongest effect in the amygdala ($z = 5.12$, $P < 0.004$ FDR) (25, 4, −23; 0.5% per year). These findings highlight that myelin-related MT increase in both cortical and subcortical areas is a marked feature of a transition from adolescence to adulthood, and conforms to a pattern that suggests that both local and inter-regional fiber projections are involved in this process.

Association between macrostructural and microstructural development. The observed developmental increase of myelin-sensitive MT exhibited overlapping topographies with macrostructural GM shrinkage (with the exception of the hippocampus) and WM expansion (Fig. 2a; see also Supplementary Fig. 4a–c and Supplementary Table 2 for macrostructural results). This raises the question of how macrostructural volume change precisely relates to development of our myelin marker MT. A positive association of changes in MT and WM volume ($r = 0.09 \pm 0.05$ (mean ± s.d.), $t = 453$, $P < 10^{-15}$) (Fig. 2b,c) supports the notion that myelination is linked to the observed changes in macrostructural volume. This notion is predicted by an assumption that increased myelination leads to an expansion in WM volume[23]. The relatively modest, but consistent, effect size is partially explained by the fact that we only investigated the purely developmental associations and controlled for potentially confounding effects. However, our findings leave open the possibility that there might be additional microstructural factors driving the change in WM macrostructure.

The voxel-wise analysis in GM revealed a more complex association between macrostructural development and myelination (Fig. 2b,c). We observed that the association depended on where a voxel is located in the tissue. An overall profile of consistently negative correlations (albeit relatively small) in GM zones close to the WM boundary (0–2 mm from the GM/WM boundary: $t = 300$, $P < 10^{-15}$) suggest that developmental myelination may lead to a 'whitening' of GM, which in turn is likely to drive partial volume effects that are evident in a shrinkage of GM volume[23,24]. This means that a decline in GM volume in deep layers during adolescence

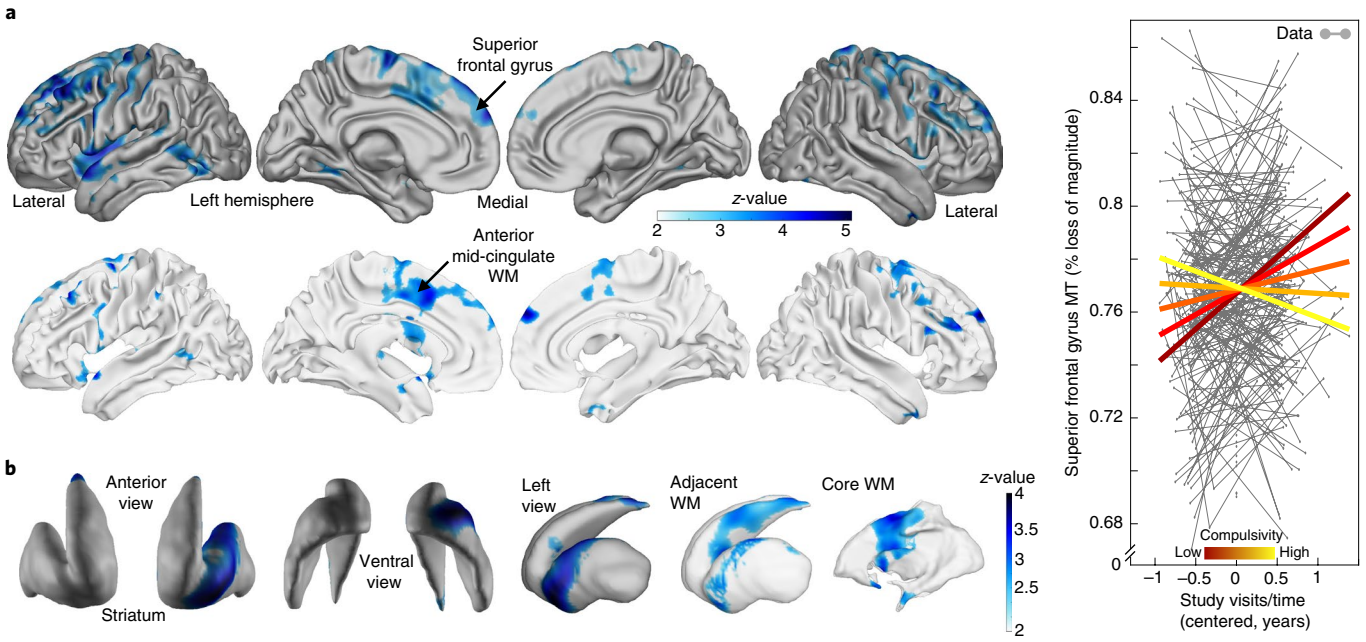

Fig. 3 | Compulsivity is related to altered frontostriatal MT growth. Longitudinal developmental changes in our myelin marker are reduced in subjects exhibiting high compulsivity. **a**, Aggregate compulsivity score is related to a decreased rate of change of MT in the dorsolateral frontal GM (upper panel; statistical *z*-maps testing for negative visit/time by compulsivity interaction, $P<0.05$, FDR- and bootstrapping-corrected; Supplementary Table 3, one-sided Wald-test, $n=452/246$ scans/subjects; these details also apply to **b**; 50.4% female). This effect is also seen in adjacent WM, centered around cingulate cortex (bottom panel; blue shading depicts negative visit/time by compulsivity interactions). In the plot of a longitudinal model for MT over visits/time, varying subject's compulsivity, subjects with higher compulsivity scores (light yellow) compared with subjects with low scores (dark red) express significantly lower MT rates of change over visits (colored lines in the map indicate the interaction effect). **b**, The slowing in cortical myelin-related growth is mirrored by decreased developmental growth in the subcortical ventral striatum and the adjacent WM. These findings indicate that young people with high compulsive traits express slower maturational myelin-related changes in a frontostriatal network comprising the cingulate cortex and ventral striatum.

may well be driven by an increase in myelination within these same areas. This negative association reduced as the distance from the WM boundary increased (Pearson $r=0.3$, $P<10^{-15}$) (Fig. 2c, lower right panel). This suggests that ongoing myelination in superficial layers (that is, close to the outer surface of the brain) may contribute to an attenuated volume reduction and implies that developmental macrostructural change is the result of complex microstructural processes.

Compulsivity linked to reduced developmental increase in cingulate, dorsolateral and striatal MT. We next tested whether individual differences in the expression of symptoms indicative of obsessive–compulsive traits were associated with distinct developmental trajectories of myelin-sensitive MT. We employed a dimensional approach exploiting the heterogeneity within this otherwise healthy community sample. We computed a compound score (first principal component, Supplementary Fig. 1a–f) from the two established obsessive–compulsive symptom questionnaire results[25,26] available in our sample to aggregate a common score to index meaningful variation (Supplementary Fig. 1). Top-loading items on this score (subsequently called 'compulsivity') reflect compulsive behaviors, such as checking, and it was strongly aligned with total scores on our obsessive–compulsive questionnaires (Pearson $r>0.8$).

Assessing how compulsivity is related to individual myelination over time, we found that our compulsive measure was linked to altered MT growth primarily in frontal areas, with significant clusters in the dorsolateral and dorsomedial frontal cortices, both in cortical GM and adjacent superficial WM (Fig. 3a; Supplementary Table 3). These were centered around superior frontal gyrus (GM: $z=4.87$, $P=0.009$ FDR (−23, 34, 49); WM: $z=4.28$, $P<0.05$ FDR (−24 −4 64)) and anterior mid-cingulate (GM: $z=4.1$, $P=0.009$ FDR (18, 1, 58); WM: $z=3.74$, $P<0.05$ FDR (−25, 1, 37)). Importantly, more compulsive subjects showed reduced MT growth compared with less compulsive subjects. A similar pattern was seen in the left ventral striatum ($z=3.9$, $P=0.018$ FDR (−22, 14, −9)) and adjacent WM ($z=4.2$, $P=0.027$ FDR (21, −9, 25)) (Fig. 3b). Intriguingly, the locations of reduced MT development were spatially centered in the cingulate and ventral striatum, and this regional focus aligns with a specific frontostriatal loop described in primate anatomical tracing studies[27]. This alignment with a well-described anatomical circuit suggests that compulsivity may relate to attenuated myelin-related developmental growth in this cingulate–striatal loop[13].

Reduced inferior prefrontal maturational changes in impulsivity. We next examined whether a common heterogeneity in impulsivity (as assessed using total scores from the Barratt impulsiveness scale (BIS); Supplementary Fig. 1f) is linked to individual growth of the myelin marker. In examining this linkage, we opted to use a questionnaire measure over task-based measures of impulsivity because the former has been found to be more reliable (see refs. [28–32] for detailed discussions). This is supported by results from our subsample study[33] ($n=63$), with a BIS total re-test reliability of $r=0.76$ (1 year of follow-up) and a reflection impulsivity decision parameter[34] reliability of $r=0.16$ (6 months of follow-up). Thus, this questionnaire reflected a stable trait that is more likely to be linked to structural development.

We found that impulsivity was associated with reductions in adolescent MT growth, with a strong focus on frontal areas encompassing lateral and medial prefrontal areas, both within GM and adjacent WM (subcortical effects shown in Supplementary Fig. 5a).

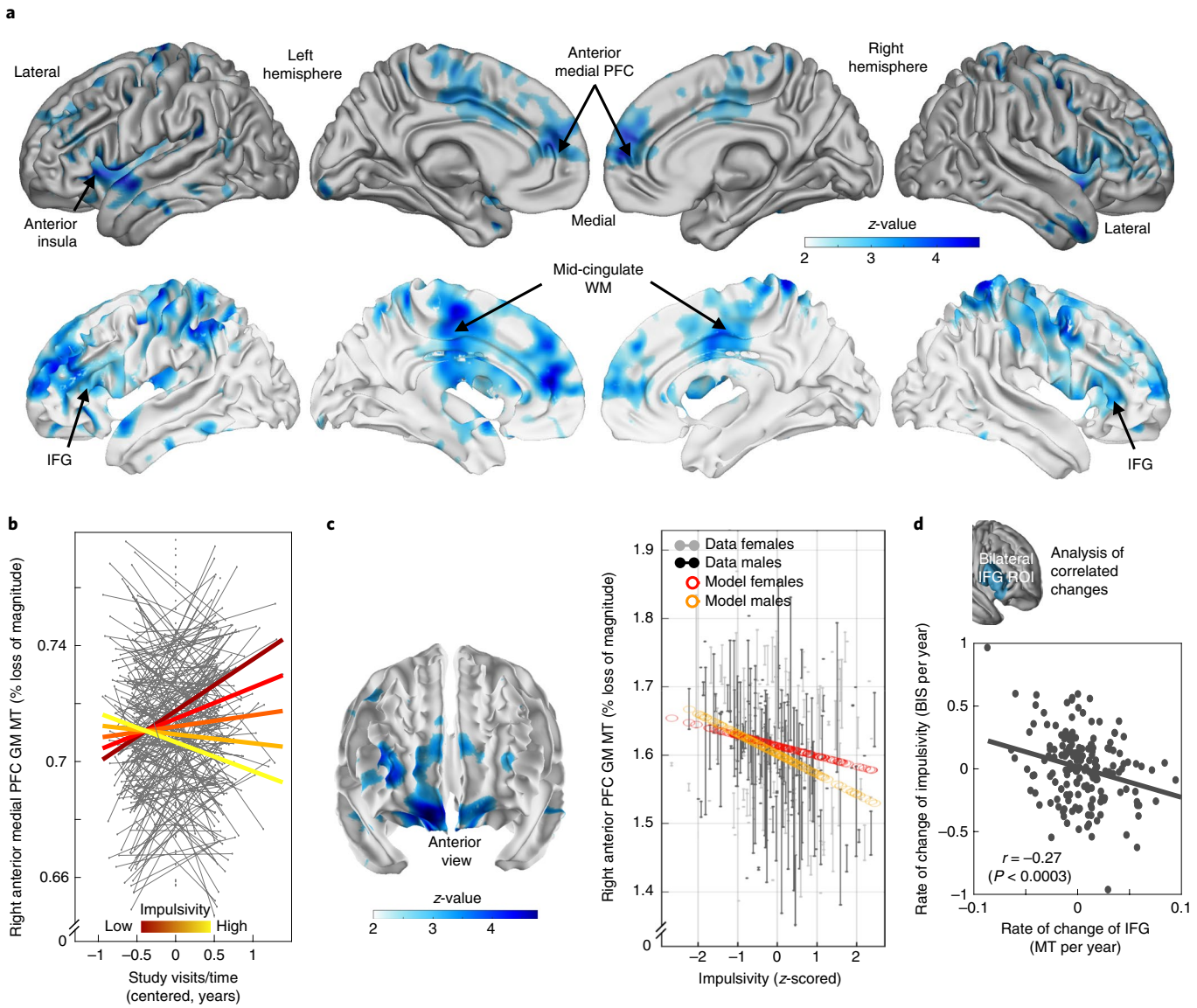

Fig. 4 | Decreased frontal growth in myelin-sensitive MT in impulsivity. The myelin marker (MT) in the frontal lobe is linked to impulsivity traits. **a**, Impulsivity is associated with reduced growth of MT in lateral (inferior and middle frontal gyrus), medial prefrontal areas, motor and premotor and parietal areas in both GM (top) and adjacent WM (bottom), depicting statistical *z*-maps testing for negative time/visit by impulsivity interactions ($P < 0.05$ FDR- and bootstrapping-corrected (see Supplementary Table 4), one-sided Wald-test, $n = 497/288$ scans/subjects, 51.7% female; details also applicable to **b** and **c**). **b**, Plot showing the longitudinal model for MT over study visits, varying subjects' impulsivity. Subjects with higher impulsivity (light yellow), compared with subjects exhibiting low scores (dark red), express significantly less MT increase over visits (colored lines in the chart indicate the interaction effect). **c**, Subjects exhibiting more impulsivity show a local decrement in the baseline myelin marker (peak middle frontal gyrus, $P < 0.05$, FDR- and bootstrapping-corrected; see Supplementary Table 5) in the lateral and orbitofrontal areas (fixed for other covariates: for example, time/visits, mean age of subject, sex). Right: the plot of MT in this peak voxel over impulsivity (*x* axis, *z*-scored) and with adjusted data (gray/black) and model predictions (red/orange, effects of interest: intercept, impulsivity, sex by impulsivity). **d**, The bilateral IFG shows both a reduced myelination process for higher impulsivity (as shown in **a** and **b**) and a reduced growth rate that is more strongly expressed in subjects who manifest an accentuated impulsivity increase over study visits. That is, subjects who manifest an even more restricted growth in myelin become more impulsive (Pearson's correlation and *P* values from corresponding *t*-distribution based on $n = 188$ independent subjects with available follow-up scans). BIS, Barratt impulsiveness scale; ROI, region of interest; PFC, prefrontal cortex.

These center around lateral prefrontal area, including the inferior frontal gyrus (IFG) (GM: $z = 4.65$, $P = 0.031$ FDR (−48, 13, −4); WM: $z = 4.38$, $P = 0.015$ FDR (−27, 39, −2)) and medial prefrontal cortex (GM: $z = 4.13$, $P = 0.031$ (15 58 18); WM: $z = 3.69$, $P = 0.015$ (−12, 47, 20)) (Fig. 4a, Supplementary Table 4).

The above findings suggest that while impulsivity and compulsivity are both linked to reduced myelin-related growth in prefrontal areas, these alterations exhibit peak expression in distinct anatomical regions. That is, the cingulate and dorsolateral versus the inferior lateral and medial prefrontal cortex (for a direct comparison see Supplementary Fig. 6). Interestingly, both compulsivity and impulsivity showed reduced growth in the anterior insula (Supplementary Fig. 6), possibly expressing a common, transdiagnostic vulnerability.

We next investigated development-independent levels of myelination in impulsivity, which may indicate myelin-related

differences that emerged before the commencement of our study. This is important because a pre-existing 'hyper-myelination' with the reduced ongoing growth would suggest a normalization process during adolescence. Conversely, a 'hypo-myelination' before adolescence onset would imply that deficient myelination was further accentuated during adolescence. We found a main effect of impulsivity evident in hypo-myelination across several, primarily anterior prefrontal, brain areas, including the IFG (Fig. 4c; Supplementary Fig. 5b; Supplementary Table 5). An overlap between these baseline effects and areas showing reduced ongoing growth suggests that for impulsivity, a gap in myelination may exist before adolescence, with this gap widening further during transition to adulthood. The same effects were found when analyzing across the entire prefrontal cortex, where a reduced MT growth was linked to both compulsivity ($t(421) = 1.99$, $P = 0.047$) and impulsivity ($t(421) = -2.80$, $P = 0.005$). Conversely, a developmental baseline hypo-myelination in impulsivity ($t(474) = 2.30$, $P = 0.022$) was further accentuated during late adolescence development (no such effect was found for compulsivity: $t(427) = 1.03$, $P = 0.30$) (Supplementary Fig. 7a,b).

Finally, we examined how MT changes related to the development of impulsivity traits. Although we did not see age-related changes in impulsivity across the entire group, there was substantial variability within individuals (Supplementary Fig. 1). We therefore investigated whether myelin growth in the IFG, a key region previously implicated in impulsivity[15], related to ongoing changes in impulsivity. We found that a change in IFG MT values was negatively associated with impulsivity change (Pearson $r = -0.27$, $P < 0.0003$; Fig. 4d), indicating that individuals with the least ongoing myelin growth had worsening impulsivity over the course of the study (irrespective of other covariates, such as baseline impulsivity or age). Similar effects were also seen in the prefrontal cortex following a voxel-wise analysis (Supplementary Fig. 7c).

Discussion

Myelin enables fast and reliable communication within and between neuronal populations[35,36]. Using a longitudinal, repeated-measures MRI scanning design in a developmental sample, we provide in vivo evidence that myelination extends into adulthood, as evident in a pronounced myelin-related whole-brain MT increase. We found that the macrostructural growth pattern closely resembles that expressed in our myelin marker. The positive association between these measures in WM suggests that changes in macrostructural volume are, at least in part, driven by myelination. In GM, depth-dependent associations suggest that reductions in macrostructural volume in adolescence are the result of multiple microstructural processes. In superficial layers, ongoing myelination seems to attenuate the impact of a pruning effect, leading to an apparent slowing in the decline in GM volume. In deeper layers, close to the GM/WM boundary, ongoing myelination appears to contribute to an inflated estimate of volume reduction, with a myelin-induced whitening of GM resulting in a misclassification of GM voxels (that is, partial volume effects[23]), leading to an apparent volume reduction. This observation builds on recent findings from cross-sectional studies in which age-related myelin increases occur in deep layers[7,24]. Moreover, this result implies that developmental neuroimaging that utilize markers sensitive to specific microstructural processes[17] can provide more precise accounts of the likely mechanisms underlying adolescent and early adult brain development.

Critically, we found that individual differences in myelin-related MT growth during development are linked to common heterogeneity in compulsivity and impulsivity within an otherwise healthy sample. Both compulsivity and impulsivity were associated with reduced MT growth, and this reduction was almost exclusively present in frontostriatal areas. In compulsivity, reduced MT growth was primarily expressed in dorsomedial and dorsolateral frontal regions as well as the ventral striatum. Conversely, impulsivity was more tightly linked to reduced MT growth in lateral and medial prefrontal regions. It is worth noting that variability in compulsivity and impulsivity does not reflect clinical impairment in this healthy sample[37]. Our findings build on results from previous animal and patient studies that implicate lateral and medial prefrontal regions in attention-related functions[38] and attention-deficit/hyperactivity disorder[15,39]. It is also noteworthy that the regions implicated in compulsivity have been reported to show altered function in OCD[40,41] and constitute prime targets for invasive OCD treatments and interventions[42,43]. Critically, our finding that reduced myelin growth is linked to compulsivity suggests that differences in structural variables of the brain may not prevail during childhood (or only to a minor extent), but emerge during adolescence as a result of aberrant developmental processes.

Embracing a longitudinal approach, as in this study allows us to pose distinct questions regarding brain development. In relation to impulsivity and compulsivity, we can ask how a stable trait is related to longitudinal change as well as baseline myelination differences, whereby the latter is more indicative of influences emerging before recruitment into our study. In the case of impulsivity, we found that ongoing growth occurred in regions similar to those that also express a difference in baseline myelination, advocating the presence of a pre-existing myelination gap in impulsivity that further expands during adolescence. This suggests that the mechanisms underlying impulsivity have long-lasting effects on brain development, possibly affecting myelination trajectories before adolescence onset and with lasting effects into adulthood.

An extension of the approach outlined above is to ask how ongoing changes in compulsivity and impulsivity relate to ongoing brain maturation (that is, correlated change). Strikingly, we found that changes in growth in the IFG were indicative of changes in impulsivity. Subjects who showed worsening of their impulsivity were also those who showed the least maturational myelin-related increase in the IFG. Thus, during the transition to early adulthood, even though impulsivity traits as a whole do not change at a population level, individual psychiatric risk trajectories show meaningful variation, and this in turn is reflected in specific patterns of brain maturation.

In our study, we adopted a broad definition of impulsivity and compulsivity traits yet found links to myelin growth. This suggests that reduced myelin-related growth in these areas may represent a developmental feature shared across multiple cognitive and/or genetic endophenotypes. This also implies that more refined cognitive endophenotyping might yield spatially more defined developmental effects[44–46]. Compulsivity and impulsivity showed little overlap in our sample, and this relative independence was also reflected in their impact on distinct frontostriatal brain regions (with the exception of the insula, which showed a common trend of growth reduction). These data leave open the possibility of genetic pleiotropy, meaning that a shared genetic factor may drive both myelination and impulsivity/compulsivity, without a direct causal influence between brain and trait expression[47]. However, our correlated change finding that ongoing myelination in the IFG is directly related to how impulsivity evolves over time advocates for the possibility of a direct relationship between myelin-related maturation and impulsivity.

Variability in trait dimensions, such as compulsivity and impulsivity, are often related to other variables known to affect brain structure. We examined how potential confounding factors, such as subject movement during scanning (Supplementary Fig. 8a–f), alcohol consumption[45,46], recreational drug use, socioeconomic status, intelligence (between-subject differences and within-subject changes; Supplementary Fig. 9a–c) or ethnicity, affected the link between compulsivity and impulsivity and MT growth. Importantly, none of these factors accounted for the observed effects (Supplementary Fig. 9d).

A challenge for human neuroscience is to determine the cellular mechanisms that underlie macrostructural changes in vivo[48]. This is of particular importance for developmental neuroscience for which longitudinal, repeated-measures approaches are critical for understanding brain development[22]. Our focus in this study of using a MT saturation protocol as a proxy for myelin content is rooted in evidence of its sensitivity to myelin and related macromolecules[17], as well as the fact that this measure is more robust against instrumental biases[20]. There is also evidence for a strong relationship between MT and myelin as measured in histological studies[18,19], and we have previously shown that MT is linked to myelin gene expression[7]. Our longitudinal findings support the importance of MT as a myelin marker, with sensitivity for individual differences. We show that myelin-related effects are expressed in both cortical GM and adjacent WM, but more pronounced in the former, as also found in ex vivo studies[4]. Taken together, our findings suggest that MT is an important, albeit imperfect, indicator of myelin.

The transition to adulthood is a particularly vulnerable stage for the emergence of psychiatric illness[10]. Our findings suggest that variability in the expression of compulsivity and impulsivity is tied to ongoing microstructural brain development. The potential of the brain to dynamically adjust its myelination patterns[49], for example, as a function of training[50], points to the potential of interventions that target specific deviant trajectories. Such interventions might offer a novel therapeutic domain to lessen a developmental vulnerability to a psychiatric disorder.

Online content

Any methods, additional references, Nature Research reporting summaries, source data, extended data, supplementary information, acknowledgements, peer review information; details of author contributions and competing interests; and statements of data and code availability are available at https://doi.org/10.1038/s41593-019-0394-3.

Received: 26 July 2018; Accepted: 25 March 2019;
Published online: 13 May 2019

References

1. Gogtay, N. et al. Dynamic mapping of human cortical development during childhood through early adulthood. *Proc. Natl Acad. Sci. USA* **101**, 8174–8179 (2004).
2. Sowell, E. R., Thompson, P. M., Holmes, C. J., Jernigan, T. L. & Toga, A. W. In vivo evidence for post-adolescent brain maturation in frontal and striatal regions. *Nat. Neurosci.* **2**, 859–861 (1999).
3. Paus, T. Growth of white matter in the adolescent brain: myelin or axon? *Brain Cogn.* **72**, 26–35 (2010).
4. Miller, D. J. et al. Prolonged myelination in human neocortical evolution. *Proc. Natl Acad. Sci. USA* **109**, 16480–16485 (2012).
5. Perrin, J. S. et al. Growth of white matter in the adolescent brain: role of testosterone and androgen receptor. *J. Neurosci.* **28**, 9519–9524 (2008).
6. Petanjek, Z. et al. Extraordinary neoteny of synaptic spines in the human prefrontal cortex. *Proc. Natl Acad. Sci. USA* **108**, 13281–13286 (2011).
7. Whitaker, K. J. et al. Adolescence is associated with genomically patterned consolidation of the hubs of the human brain connectome. *Proc. Natl Acad. Sci. USA* **113**, 9105–9110 (2016).
8. Foulkes, L. & Blakemore, S.-J. Studying individual differences in human adolescent brain development. *Nat. Neurosci.* **21**, 315–323 (2018).
9. Kessler, R. C. et al. Lifetime prevalence and age-of-onset distributions of mental disorders in the World Health Organization's World Mental Health Survey Initiative. *World Psychiatry* **6**, 168–176 (2007).
10. Paus, T., Keshavan, M. & Giedd, J. N. Why do many psychiatric disorders emerge during adolescence? *Nat. Rev. Neurosci.* **9**, 947–957 (2008).
11. McCarthy, H. et al. Attention network hypoconnectivity with default and affective network hyperconnectivity in adults diagnosed with attention-deficit/hyperactivity disorder in childhood. *JAMA Psychiatry* **70**, 1329–1337 (2013).
12. Douaud, G. et al. A common brain network links development, aging, and vulnerability to disease. *Proc. Natl Acad. Sci. USA* **111**, 17648–17653 (2014).
13. Robbins, T. W., Gillan, C. M., Smith, D. G., de Wit, S. & Ersche, K. D. Neurocognitive endophenotypes of impulsivity and compulsivity: towards dimensional psychiatry. *Trends Cogn. Sci.* **16**, 81–91 (2012).
14. de Wit, S. J. et al. Multicenter voxel-based morphometry mega-analysis of structural brain scans in obsessive–compulsive disorder. *Am. J. Psychiatry* **171**, 340–349 (2014).
15. Norman, L. J. et al. Structural and functional brain abnormalities in attention-deficit/hyperactivity disorder and obsessive–compulsive disorder: a comparative meta-analysis. *JAMA Psychiatry* **73**, 815–825 (2016).
16. Carlisi, C. O. et al. Comparative multimodal meta-analysis of structural and functional brain abnormalities in autism spectrum disorder and obsessive–compulsive disorder. *Biol. Psychiatry* **82**, 83–102 (2016).
17. Weiskopf, N., Mohammadi, S., Lutti, A. & Callaghan, M. F. Advances in MRI-based computational neuroanatomy: from morphometry to in-vivo histology. *Curr. Opin. Neurol.* **28**, 313–322 (2015).
18. Schmierer, K., Scaravilli, F., Altmann, D. R., Barker, G. J. & Miller, D. H. Magnetization transfer ratio and myelin in postmortem multiple sclerosis brain. *Ann. Neurol.* **56**, 407–415 (2004).
19. Turati, L. et al. In vivo quantitative magnetization transfer imaging correlates with histology during de- and remyelination in cuprizone-treated mice. *NMR Biomed.* **28**, 327–337 (2015).
20. Callaghan, M. F., Helms, G., Lutti, A., Mohammadi, S. & Weiskopf, N. A general linear relaxometry model of R1 using imaging data. *Magn. Reson. Med.* **73**, 1309–1314 (2015).
21. Campbell, J. S. W. et al. Promise and pitfalls of g-ratio estimation with MRI. *NeuroImage* **182**, 80–96 (2018).
22. Raz, N. & Lindenberger, U. Only time will tell: cross-sectional studies offer no solution to the age–brain–cognition triangle: comment on Salthouse (2011). *Psychol. Bull.* **137**, 790–795 (2011).
23. Paus, T. Mapping brain maturation and cognitive development during adolescence. *Trends Cogn. Sci.* **9**, 60–68 (2005).
24. Natu, V. S. et al. Apparent thinning of visual cortex during childhood is associated with myelination, not pruning. Preprint at *bioRxiv* https://doi.org/10.1101/368274 (2018).
25. Burns, G. L., Keortge, S. G., Formea, G. M. & Sternberger, L. G. Revision of the padua inventory of obsessive compulsive disorder symptoms: distinctions between worry, obsessions, and compulsions. *Behav. Res. Ther.* **34**, 163–173 (1996).
26. Foa, E. B. et al. The obsessive–compulsive inventory: development and validation of a short version. *Psychol. Assess.* **14**, 485–496 (2002).
27. Haber, S. N. Corticostriatal circuitry. *Dialogues Clin. Neurosci.* **18**, 7–21 (2016).
28. Palminteri, S. & Chevallier, C. Can we infer inter-individual differences in risk-taking from behavioral tasks? *Front. Psychol.* **9**, 2307 (2018).
29. Pedroni, A. et al. The risk elicitation puzzle. *Nat. Hum. Behav.* **1**, 803 (2017).
30. Frey, R., Pedroni, A., Mata, R., Rieskamp, J. & Hertwig, R. Risk preference shares the psychometric structure of major psychological traits. *Sci. Adv.* **3**, e1701381 (2017).
31. Moutoussis, M. et al. Change, stability, and instability in the Pavlovian guidance of behaviour from adolescence to young adulthood. *PLoS Comput. Biol.* **14**, e1006679 (2018).
32. Shahar, N. et al. Improving the reliability of model-based decision-making estimates in the two-stage decision task with reaction-times and drift-diffusion modeling. *PLoS Comput. Biol.* **15**, e1006803 (2019).
33. Kiddle, B. et al. Cohort profile: The NSPN 2400 Cohort: a developmental sample supporting the Wellcome Trust NeuroScience in Psychiatry Network. *Int. J. Epidemiol.* **47**, 18–19g (2018).
34. Moutoussis, M., Bentall, R. P., El-Deredy, W. & Dayan, P. Bayesian modelling of Jumping-to-Conclusions bias in delusional patients. *Cognit. Neuropsychiatry* **16**, 422–447 (2011).
35. Virchow, R. Ueber das ausgebreitete Vorkommen einer dem Nervenmark analogen Substanz in den thierischen Geweben. *Arch. Für Pathol. Anat. Physiol. Für Klin. Med.* **6**, 562–572 (1854).
36. Bunge, R. P. Glial cells and the central myelin sheath. *Physiol. Rev.* **48**, 197–251 (1968).
37. Holmes, A. J. & Patrick, L. M. The myth of optimality in clinical neuroscience. *Trends Cogn. Sci.* **22**, 241–257 (2018).
38. Rubia, K. 'Cool' inferior frontostriatal dysfunction in attention-deficit/hyperactivity disorder versus 'hot' ventromedial orbitofrontal-limbic dysfunction in conduct disorder: a review. *Biol. Psychiatry* **69**, e69–e87 (2011).
39. Hauser, T. U. et al. Role of the medial prefrontal cortex in impaired decision making in juvenile attention-deficit/hyperactivity disorder. *JAMA Psychiatry* **71**, 1165–1173 (2014).
40. Hauser, T. U. et al. Increased fronto-striatal reward prediction errors moderate decision making in obsessive–compulsive disorder. *Psychol. Med.* **47**, 1246–1258 (2017).
41. Gillan, C. M. et al. Functional neuroimaging of avoidance habits in obsessive–compulsive disorder. *Am. J. Psychiatry* **172**, 284–293 (2015).

42. Dougherty, D. D. et al. Prospective long-term follow-up of 44 patients who received cingulotomy for treatment-refractory obsessive–compulsive disorder. *Am. J. Psychiatry* **159**, 269–275 (2002).
43. Figee, M. et al. Deep brain stimulation restores frontostriatal network activity in obsessive–compulsive disorder. *Nat. Neurosci.* **16**, 386–387 (2013).
44. Boedhoe, P. S. W. et al. Distinct subcortical volume alterations in pediatric and adult OCD: a worldwide meta- and mega-analysis. *Am. J. Psychiatry* **174**, 60–69 (2016).
45. Whelan, R. et al. Adolescent impulsivity phenotypes characterized by distinct brain networks. *Nat. Neurosci.* **15**, 920–925 (2012).
46. Holmes, A. J., Hollinshead, M. O., Roffman, J. L., Smoller, J. W. & Buckner, R. L. Individual differences in cognitive control circuit anatomy link sensation seeking, impulsivity, and substance use. *J. Neurosci.* **36**, 4038–4049 (2016).
47. Pingault, J.-B. et al. Using genetic data to strengthen causal inference in observational research. *Nat. Rev. Genet.* **19**, 566–580 (2018).
48. Lerch, J. P. et al. Studying neuroanatomy using MRI. *Nat. Neurosci.* **20**, 314–326 (2017).
49. Franklin, R. J. M. & Ffrench-Constant, C. Remyelination in the CNS: from biology to therapy. *Nat. Rev. Neurosci.* **9**, 839–855 (2008).
50. Sampaio-Baptista, C. et al. Motor skill learning induces changes in white matter microstructure and myelination. *J. Neurosci.* **33**, 19499–19503 (2013).

Acknowledgements

A Wellcome Trust Cambridge–UCL Mental Health and Neurosciences Network grant (095844/Z/11/Z) supported this work. R.J.D. holds a Wellcome Trust Investigator Award (098362/Z/12/Z). The UCL–Max Planck Centre is a joint initiative supported by UCL and the Max Planck Society. T.U.H. is supported by a Wellcome Sir Henry Dale Fellowship (211155/Z/18/Z), a grant from the Jacobs Foundation, the Medical Research Foundation, and a 2018 NARSAD Young Investigator grant (27023) from the Brain & Behavior Research Foundation. M.M. receives support from the UCLH NIHR BRC. P.F. is in receipt of a National Institute for Health Research (NIHR) Senior Investigator Award (NF-SI-0514-10157), and was in part supported by the NIHR Collaboration for Leadership in Applied Health Research and Care North Thames at Barts Health NHS Trust. E.T.B. is in receipt of a NIHR Senior Investigator Award, and was in part supported by the NIHR Cambridge Biomedical Research Centre. The Wellcome Centre for Human Neuroimaging is supported by core funding from the Wellcome Trust (203147/Z/16/Z). The authors thank R. Davis and FIL IT support for making large sample analysis feasible and more efficient. Thanks are also given to G. Prabhu, and to specific experts for input in relation to applied and technical methods, particularly R. Dahnke, W. Penny, G. Ridgway, M. Callaghan, N. Weiskopf, B. Draganski, J. Ashburner, C. Gaser, G. Flandin, T. Nichols, B. Guillaume, J. Bernal-Rusiel, M. Völkle, C. Driver, A. Brandmeier, F. Dick, M. Betts, G. J. Will and R. Kievit. Finally, G.Z. thanks E. Düzel for support at the DZNE. The views expressed are those of the authors and not necessarily those of the NHS, the NIHR or the Department of Health and Social Care.

Author contributions

E.T.B., I.M.G., P.F., P.B.J., NSPN Consortium members, M.M., T.U.H. and R.J.D. designed the experiments. G.Z., T.U.H. and NSPN Consortium members performed the experiments and analyzed the data. G.Z., T.U.H., U.L. and R.J.D. wrote the paper.

Competing interests

E.T.B. is employed half of the time by the University of Cambridge and half of the time by GlaxoSmithKline and holds stock in GlaxoSmithKline. All other authors declare no competing interests.

Additional information

Supplementary information is available for this paper at https://doi.org/10.1038/s41593-019-0394-3.

Reprints and permissions information is available at www.nature.com/reprints.

Correspondence and requests for materials should be addressed to G.Z. or T.U.H.

Journal peer review information: *Nature Neuroscience* thanks Lars Tjelta Westlye and other anonymous reviewer(s) for their contribution to the peer review of this work.

Publisher's note: Springer Nature remains neutral with regard to jurisdictional claims in published maps and institutional affiliations.

Methods

Study design and participants. The NSPN study[33] used an accelerated longitudinal design to investigate variability in compulsivity and impulsivity traits and brain maturation during adolescence and early adulthood. Participants were recruited in London and Cambridgeshire, UK, from schools, colleges, primary care services and through advertisements. Subjects were sampled in five age bins (14–15 years, 16–17 years, 18–19 years, 20–21 years and 22–24 years), with roughly balanced numbers (overall mean (s.d.) age of 19.45 (2.85) years). Each age bin was balanced for sex and ethnicity (relative to the local population). From the 2,406 participants who took part in the study and who filled out sociodemographic information and questionnaires at least once, 318 healthy subjects (~60 subjects per age bin) participated in the MRI group. Subjects with self-reported pervasive neurological, developmental or psychiatric disorders were excluded from the study. After rigorous visual quality control and excluding 10% of scans with highest during-scan motion (see Supplementary Fig. 8 for details), of all 558 processed imaging datasets, 61 scans from 30 subjects had to be discarded due to severe artifacts. We finally analyzed 497 available brain scans from 288 (149 female) healthy individuals that passed rigorous quality control. In particular, data from 100, 167 and 21 subjects with one, two or three visits per person were available, with a mean (s.d.) follow-up interval of 1.3 (0.32) years between the first and last visit. The study was approved by the Cambridge Central Research Ethics Committee (12/EE/0250), and all participants (if <16 years old, also their legal guardian) gave written informed consent.

Assessing compulsivity and impulsivity. To examine the effects of compulsivity and impulsivity traits on myelin development, we analyzed psychometric questionnaires that were handed out to the participants over the course of the study. A detailed description of the assessment waves and the overall structure of the NSPN study is provided elsewhere[33]. As an index of impulsivity, we used the BIS[51] total score, a well-established and calibrated measure of general impulsivity. To assess compulsivity, we built a composite score (using principal component analysis, see Supplementary Information) from two established obsessive–compulsive questionnaires that were available in this study: the revised Obsessive–Compulsive Inventory (OCI-R)[26] and the revised Padua Inventory (PI-WSUR)[25] (Supplementary Fig. 1a–e).

Questionnaires were assessed at several times throughout the study. The BIS questionnaire was completed at home by participants on up to three occasions (~1 year between assessments), with the first assessment wave taking place before initial scanning. PI-WSUR questionnaires were also completed at home during the second and third assessment waves. OCI-R questionnaires were assessed on the day of the second MRI scan. Per construction, the considered psychometric questionnaires aim at measuring stable subject-specific traits, but these constructs could also change over the course of this longitudinal study. In our sample, linear mixed-effects (LME) modeling (see Supplementary Information) revealed that both indices did not substantially change during the study period while accounting for covariates and confounding factors, which motivated our use of aggregated scores (LME intercepts) for most of the subsequent MRI analyses on impulsivity. Compulsivity and impulsivity trait measures showed a weak correlation (Pearson $r=0.119$) in the large behavioral sample, supporting a notion of relatively independent dimensions (less than 1.4% shared variance; Supplementary Fig. 1).

MRI data acquisition and longitudinal preprocessing. Brain scans were acquired using the multi-echo FLASH MPM protocol[52] on three 3T Siemens Magnetom TIM Trio MRI systems located in Cambridge and London, UK. Comparability among scanners was assessed before study onset (for more details, see ref. [33]), and differences among scanners were accounted for by adding scanner as a covariate in our analyses. Isotropic 1-mm MT maps were collected to quantify local changes in GM and adjacent WM, and all image processing was performed using SPM12 (Wellcome Centre for Human Neuroimaging, London, UK, http://www.fil.ion.ucl.ac.uk/spm), the h-MRI toolbox for SPM[53,54] (www.hmri.info), the computational anatomy toolbox (CAT; http://www.neuro.uni-jena.de/cat/) and custom-made tools (see Code availability).

MT saturation maps provide semiquantitative maps for myelin and related macromolecules, and correlate highly with myelin content in histological studies[18,19]. MT shows high sensitivity to actual microstructural changes in myelin and thus overcomes limitations of previous methods such as diffusion tensor imaging, which indirectly measures microstructural change by assessing diffusivity[55]. MT saturation was also found to be more robust than earlier protocols such as MT ratio[20]. This is important because myelin patterns are used to define brain anatomy and for subdividing brain structures[56,57].

Since longitudinal neuroimaging is prone to artifacts due to inconsistencies in registration and scanners, and age-related deformations of the brains, we developed advanced processing pipelines to detect the changes of interest and to achieve unbiased results. To assess the microstructural myelin-related MT changes during development, we used a longitudinal processing pipeline with the following steps (Supplementary Fig. 2a). To normalize images, we performed a symmetric diffeomorphic registration for longitudinal MRI[58]. The optimization is realized within one integrated generative model and provides consistent estimates of within-subject brain deformations over the study period and a midpoint image for each subject. The midpoint image is subsequently segmented into GM, WM and cerebrospinal fluid using CAT. MT maps from all time points were then normalized to MNI space using geodesic shooting[59,60] and spatially smoothed preserving GM/WM tissue boundaries[54]. Maps were also manually and statistically quality checked using a proxy for during-scan motion (Supplementary Fig. 8) and covariance-based sample homogeneity measures (as implemented in CAT). Finally, we constructed masks for both GM and adjacent WM using anatomical atlases for subsequent analyses (illustrated in Supplementary Fig. 2b).

To relate these quantitative (voxel-based quantification (VBQ)) to more conventional metrics (that is, voxel-based morphometry (VBM)), we normalized tissue segment maps to account for existing differences and ongoing changes of local volumes using within- and between-subject modulation. The obtained maps were spatially smoothed (6-mm full width at half maximum). All analyses were conducted in voxel space and then projected onto surface space for illustration purposes. Voxel-wise result maps can be inspected online (see Data availability).

In this paper, we focused on the developmental VBQ analysis of myelin-sensitive MT. Since, to our knowledge, this is one of the first longitudinal studies to use this marker, effects of demographics (time and number of visits (hereafter designated time/visits), age and sex) as well as impulsivity and compulsivity were considered on the whole-brain level. The analyses were particularly aimed at exploring MT trajectories in GM and the adjacent superficial WM tissue. To define disjunct but adjacent GM and WM regions for voxel-based analysis in the MNI template space, the GM and WM tissue classes of the template were thresholded at 0.5, resulting in an approximately symmetric GM/WM boundary. That is, with roughly 0.5 probability for each tissue class for voxels on the boundary (shown in Fig. 2). The resulting (non-overlapping) canonical GM and WM tissue masks are not expected to be biased toward either GM or WM and thus avoid overestimation or underestimation on both tissue classes. The subcortical GM and WM masks were computed analogously.

Longitudinal design specification, MT image and statistical analyses. In this study, we employed a longitudinal observational design to examine myelin-related MT development in late adolescence and early adulthood. Traditional cross-sectional approaches employ between-subject measures to study age-related differences rather than within-subject changes. These approaches can be affected by biases[61], such as cohort differences[62,63] or selection bias[64], and typically require additional assumptions such as (1) the age-related effect in the sample is an unbiased estimate of the group-level average of individual within-subject effects of time or (2) all subjects change in the same way. Here, we followed recent analysis recommendations[65], taking advantage of the accelerated longitudinal design in which we studied separately (in one joint model) (1) how the individual brain changes over time/visits (from baseline to follow up) and (2) how it varies with mean age of different subjects in the study and their interaction. To do so, we used the accurate and efficient sandwich estimator (SwE)[65] method for voxel-based longitudinal image analysis (http://www.nisox.org/Software/SwE; see also Supplementary Information). Similar to common cross-sectional general linear modeling approaches, this so-called marginal model describes expected variability as a function of predictors in a design matrix, while additionally accounting for correlations due to repeated measurements and unexplained variations across individuals as an enriched error term (illustrated in Supplementary Fig. 2b).

In our developmental analyses, we focused on the factors time/visits and mean age of the individual (over all visits). Moreover, to investigate whether, and how, compulsivity and impulsivity traits are related to brain trajectories and altered growth, we enriched the models by adding a main effect of trait (compulsivity and impulsivity) as well as their interaction with change over time/visits. The latter metric allowed us to assess how MT growth is associated with compulsivity and impulsivity traits (for example, lower MT growth in high compulsives), whereas the former indicates how a trait relates to overall MT differences across individuals, independent of all other covariates (including time, mean age of a subject over all scans, sex). Unless specifically mentioned, all analyses were performed in a dimensional manner directly using the trait scores of the subjects rather than comparing split groups. Notably, in addition to including effects of time/visit, mean age of subject (hereafter denoted age_mean), and compulsivity and impulsivity traits, all models were tested for the following indications of effects: (1) other relevant demographic factors, especially sex and socioeconomic status (as measured using the national poverty index[66]); (2) effects of motion during scanning, as indicated by a standard deviation of R2* exponential decay residuals in WM areas (see Supplementary Information and Supplementary Fig. 8a–c); (3) nonlinearites (accelerations and deceleration) of brain changes (across the study age range) and age-related trajectories, especially using time by age_mean interactions, and quadratic and cubic effects of age_mean; and (4) all first-order interactions among all previous covariates. All image analyses, if not reported differently, were based on one-sided Wald tests implementing the research questions (such as hypothesized developmental growth or trait-related reduction) described above. More detailed notes on longitudinal modeling and design specification can be found in the Supplementary Information.

There were no indications of substantial nonlinearities for myelin-sensitive MT (Supplementary Fig. 3d), but there were for volumes (Supplementary Fig. 4b). Demographic covariates and confounding factors (motion, total intracranial volume, scanner and socioeconomic status) were included in all models, and additional interactions of covariates were included when showing significant effects. This is intended to account for potential confounding effects of residual head-size variations induced by tissue-weighted smoothing of quantitative MT

analysis during morphometric analysis. Additionally, this allows utilization of a consistent design (and power) across modalities. We additionally examined the effects of potentially confounding covariates, such as alcohol consumption, recreational drug use, ethnicity ('white' versus 'other') and IQ, but did not find any effect on our main results (Supplementary Fig. 9d). We controlled for FDR during corrections for multiple comparisons in all image analyses. We additionally report bootstrapping-based results (Supplementary Fig. 2c; Supplementary Tables 1, 3–5). We illustrate local trajectories using model predictions based on parameters and data averaged in 6-mm spheres around peak effects. These model predictions are focused on specific effects of interest (for example, study visit or impulsivity) while the data are shown adjusting for effects of no interest (for example, other covariates and confounding factors; illustrated in Supplementary Fig. 4b).

To examine the topographical similarity of growth effects in GM and adjacent WM, we assessed the correlation between GM and nearest neighboring WM voxels (significance tested using 1,000 permutation tests).

The sample size was conceived by the NSPN Consortium during the design of this study based on the developmental studies that were available at the time[33]. We used normalization procedures (z-scoring and boxcox-transformation) for the psychometric data to align with the normality assumptions of our tests. In addition, all quantitative MRI image analyses were additionally examined using sampling methods that do not assume normality of data distributions to allow valid inference. Our study applied an observational design, and no randomization of subgroups was used. Our study design also implied that data collection and analyses were not performed blinded.

Analysis of macrostructural changes and MT–volume associations. To relate the findings from our microstructural myelin marker (MT) to traditional macrostructural markers (GM/WM volume), we performed analog analyses (using VBM[67]) as described above on traditional normalized tissue segment maps. To quantify how developmental changes of macrostructural to microstructural parameters correlate, we specified a multimodal SwE model, including all volumetric and MT scans in a joint (block-diagonal) design matrix with all covariates separately for each modality. Developmental effects within each modality were defined by respective time/visit and age_mean beta estimates of those regressors of the design matrix. After SwE model estimation, the posterior covariance of these beta parameters from volume and MT modalities were calculated and transformed into correlation values (Fig. 2b).

Assessing widespread effects of compulsivity and impulsivity. To assess the effects of development and compulsivity and impulsivity on myelin-sensitive MT across the entire frontal lobe (GM and WM separately), we used LME modeling (see Supplementary Information). In addition to assessing the effects of time/visit and time via (continuous) trait interactions, we calculated the model predictions over the study period while accounting for covariates[68]. Random-effect intercepts were included and proved optimally suited for likelihood ratio tests. Global frontal MT was analyzed separately for each dimension (shown in Supplementary Fig. 7a) and jointly with both dimensions (and their interaction) included in the design (Supplementary Fig. 7b). For both of these global models, we used discrete (median split bivariate traits: low versus high) for simplified illustration, although continuous variables were used during modeling.

Analysis of correlated changes of brain and impulsivity. To assess whether MT development was related to individual changes in impulsivity, we conducted a hypothesis-driven analysis of the bilateral IGF (anatomically defined). This LME analysis provides information about whether changes in impulsivity also reflect how quickly a brain region myelinates during the study period. The LME model used IFG MT, rates of change in IFG MT, time, their interaction, as well as the above introduced covariates as fixed effects to predict the dependent variable impulsivity score. We visualized the observed changes using simple correlations. In addition, we conducted exploratory voxel-wise correlated change analyses. Time-varying BIS scores were decomposed in purely within- and between-subject components and entered as regressors in voxel-wise SwE modeling of myelin-sensitive MT (in addition to the covariates time/visits, age_mean, sex, interactions and confounding factors; see Supplementary Information).

Analysis of MT peak effect specificity for both traits and compulsivity subtests. The voxel-based SwE analysis described above assessed whether there is region-specific growth in myelin-sensitive MT and compulsivity and impulsivity-related impairment of the ongoing myelination process. We also complemented this with a subsequent analysis of MT in observed frontostriatal peak effects (Figs. 3 and 4) and global frontal MT using LME modeling. Specifically, we were interested in the specificity of local brain trajectories associated with each or eventually both impulsivity and compulsivity traits. The fixed effects design was specified with $X=$(intercept, time/visit, time by trait interaction, trait, age_mean, sex, socioeconomic status, confounders), similar to the mass-univariate SwE models described above. We explored the potential interaction of both dimensions, in addition to separately modeling (presented in Figs. 3 and 4), a joint model was specified that included both traits simultaneously as well as their interaction (not found to be significant), and their respective interactions with time/visits. By including both effects of trait as well as their time by trait interaction, we accounted for potential baseline and rate-of-change differences related to both trait dimensions, simultaneously rendering coefficients and statistics specific for each dimension. Random effects were restricted to intercepts. The specificity of MT (averaged in 6-mm spheres around peaks observed in the voxel-based SwE analysis described above) for compulsivity and impulsivity is presented in Supplementary Fig. 6. Finally, we assessed the specificity of two available compulsivity scores, OCI-R and PI-WSUR, for the observed reduced MT growth effects using our compulsivity dimension (from principal component analysis). Thus, we explored the main effect of each subscore and time/visit interactions on local MT trajectories (averaged in 6-mm spheres of peaks presented in Fig. 3a) as detailed in Supplementary Fig. 5c.

Reporting Summary. Further information on research design is available in the Nature Research Reporting Summary linked to this article.

Data availability

Whole-brain results are available for inspection online on Neurovault (https://neurovault.org/collections/YAHZLJRW/). Data for this specific paper have been uploaded to the Cambridge Data Repository (https://doi.org/10.17863/CAM.12959) and password protected. Our participants did not give informed consent for their measures to be made publicly available, and it is possible that they could be identified from this dataset. Access to the data supporting the analyses presented in this paper will be made available to researchers with a reasonable request to openNSPN@medschl.cam.ac.uk or the corresponding authors (G.Z. and T.U.H.).

Code availability

The custom-made SPM pipeline code for longitudinal VBM and VBQ processing is provided along with the manuscript at https://github.com/gabrielziegler/gz/tree/master/nspn_mpm_prepro_code_and_example. The code aims to be transparent regarding its applied procedures, but is not intended for clinical use. It is free, but is copyrighted software distributed under the terms of the GNU General Public Licence as published by the Free Software Foundation (either version 2, or at your option, any later version). For any questions and requests please contact G.Z.

References

51. Patton, J. H., Stanford, M. S. & Barratt, E. S. Factor structure of the Barratt impulsiveness scale. *J. Clin. Psychol.* **51**, 768–774 (1995).
52. Weiskopf, N. et al. Quantitative multi-parameter mapping of R1, PD*, MT, and R2* at 3T: a multi-center validation. *Front. Neurosci.* **7**, 95 (2013).
53. Callaghan, M. F. et al. Widespread age-related differences in the human brain microstructure revealed by quantitative magnetic resonance imaging. *Neurobiol. Aging* **35**, 1862–1872 (2014).
54. Draganski, B. et al. Regional specificity of MRI contrast parameter changes in normal ageing revealed by voxel-based quantification (VBQ). *NeuroImage* **55**, 1423–1434 (2011).
55. Jones, D. K., Knösche, T. R. & Turner, R. White matter integrity, fiber count, and other fallacies: the do's and don'ts of diffusion MRI. *NeuroImage* **73**, 239–254 (2013).
56. Donahue, C. J., Glasser, M. F., Preuss, T. M., Rilling, J. K. & Van Essen, D. C. Quantitative assessment of prefrontal cortex in humans relative to nonhuman primates. *Proc. Natl Acad. Sci. USA* **115**, E5183–E5192 (2018).
57. Glasser, M. F. et al. A multi-modal parcellation of human cerebral cortex. *Nature* **536**, 171–178 (2016).
58. Ashburner, J. & Ridgway, G. R. Symmetric diffeomorphic modeling of longitudinal structural MRI. *Front. Neurosci.* **6**, 197 (2012).
59. Ashburner, J. A fast diffeomorphic image registration algorithm. *NeuroImage* **38**, 95–113 (2007).
60. Ashburner, J. & Friston, K. J. Diffeomorphic registration using geodesic shooting and Gauss–Newton optimisation. *NeuroImage* **55**, 954–967 (2011).
61. Neuhaus, J. M. & Kalbfleisch, J. D. Between- and within-cluster covariate effects in the analysis of clustered data. *Biometrics* **54**, 638–645 (1998).
62. Hoffman, L., Hofer, S. M. & Sliwinski, M. J. On the confounds among retest gains and age-cohort differences in the estimation of within-person change in longitudinal studies: a simulation study. *Psychol. Aging* **26**, 778–791 (2011).
63. Sliwinski, M., Hoffman, L. & Hofer, S. M. Evaluating convergence of within-person change and between-person age differences in age-heterogeneous longitudinal studies. *Res. Hum. Dev.* **7**, 45–60 (2010).
64. Lash, T. L., Fox, M. P. & Fink, A. K. *Applying Quantitative Bias Analysis to Epidemiologic Data* (Springer, 2009).
65. Guillaume, B. et al. Fast and accurate modelling of longitudinal and repeated measures neuroimaging data. *NeuroImage* **94**, 287–302 (2014).
66. *Personal and Household Finances* https://www.ons.gov.uk/peoplepopulationandcommunity/personalandhouseholdfinances/ (Office for National Statistics, accessed 17 October 2018).
67. Ashburner, J. & Friston, K. J. Voxel-based morphometry—the methods. *NeuroImage* **11**, 805–821 (2000).
68. Gelman, A. et al. *Bayesian Data Analysis* 3rd edn (Chapman and Hall/CRC, 2013).

nature research

Corresponding author(s): G.Ziegler & T. Hauser

Last updated by author(s): Feb 27, 2019

Reporting Summary

Nature Research wishes to improve the reproducibility of the work that we publish. This form provides structure for consistency and transparency in reporting. For further information on Nature Research policies, see Authors & Referees and the Editorial Policy Checklist.

Statistics

For all statistical analyses, confirm that the following items are present in the figure legend, table legend, main text, or Methods section.

n/a	Confirmed	
☐	☒	The exact sample size (*n*) for each experimental group/condition, given as a discrete number and unit of measurement
☐	☒	A statement on whether measurements were taken from distinct samples or whether the same sample was measured repeatedly
☐	☒	The statistical test(s) used AND whether they are one- or two-sided *Only common tests should be described solely by name; describe more complex techniques in the Methods section.*
☐	☒	A description of all covariates tested
☐	☒	A description of any assumptions or corrections, such as tests of normality and adjustment for multiple comparisons
☐	☒	A full description of the statistical parameters including central tendency (e.g. means) or other basic estimates (e.g. regression coefficient) AND variation (e.g. standard deviation) or associated estimates of uncertainty (e.g. confidence intervals)
☐	☒	For null hypothesis testing, the test statistic (e.g. *F*, *t*, *r*) with confidence intervals, effect sizes, degrees of freedom and *P* value noted *Give P values as exact values whenever suitable.*
☐	☒	For Bayesian analysis, information on the choice of priors and Markov chain Monte Carlo settings
☐	☒	For hierarchical and complex designs, identification of the appropriate level for tests and full reporting of outcomes
☐	☒	Estimates of effect sizes (e.g. Cohen's *d*, Pearson's *r*), indicating how they were calculated

Our web collection on statistics for biologists contains articles on many of the points above.

Software and code

Policy information about availability of computer code

Data collection	No software was used.
Data analysis	MATLAB 2016b (https://de.mathworks.com/products/matlab.html), SPM12 r7219 (https://www.fil.ion.ucl.ac.uk/spm/software/), hMRI toolbox for SPM (https://github.molgen.mpg.de/VBQ-toolbox-group/hMRI-Toolbox-public), CAT12 toolbox for SPM r1318 (http://www.neuro.uni-jena.de/cat/), Sandwich Estimator Toolbox for SPM r2.0.0 (http://www.nisox.org/Software/SwE/)

For manuscripts utilizing custom algorithms or software that are central to the research but not yet described in published literature, software must be made available to editors/reviewers. We strongly encourage code deposition in a community repository (e.g. GitHub). See the Nature Research guidelines for submitting code & software for further information.

Data

Policy information about availability of data

All manuscripts must include a data availability statement. This statement should provide the following information, where applicable:

- Accession codes, unique identifiers, or web links for publicly available datasets
- A list of figures that have associated raw data
- A description of any restrictions on data availability

Whole-brain results are available for inspection online on Neurovault (https://neurovault.org/collections/YAHZLJRW/). Data for this specific paper has been uploaded to the Cambridge Data Repository (https://doi.org/10.17863/CAM.12959) and password protected. Our participants did not give informed consent for their measures to be made publicly available, and it is possible that they could be identified from this data set. Access to the data supporting the analyses presented in this paper will be made available to researchers with a reasonable request to openNSPN@medschl.cam.ac.uk or the corresponding authors [G.Z., T.U.H.].

Field-specific reporting

Please select the one below that is the best fit for your research. If you are not sure, read the appropriate sections before making your selection.

☒ Life sciences ☐ Behavioural & social sciences ☐ Ecological, evolutionary & environmental sciences

For a reference copy of the document with all sections, see nature.com/documents/nr-reporting-summary-flat.pdf

Life sciences study design

All studies must disclose on these points even when the disclosure is negative.

Sample size	Imaging sample size of 300 was determined by NSPN consortium before onset of the study as a power analysis of the then (2012) available developmental studies.
Data exclusions	Available image data was visually quality checked by experts during processing and final image data underwent movement artifact removal using using R2* during-scan motion criteria with excluding 10% of worst cases. Moreover a covariance-based statistical outlier check was applied before entering analysis. Severe artifacts and outliers were excluded and motion proxy was entered as covariate during analysis. Exclusion criteria were established during the study.
Replication	We perfomed a validation study using a region-based summary statistic approach to reproduce the main finding of developmental effects and affected rates of change of growth with higher expression of psychiatric traits. Summary statistics here refers to calculating intercept and slope for each ROI and individual and modelling those in a second level model with age, sex, ses and traits as predictors. We were able to confirm the same pattern of results as presented in voxel-based Sandwich estimator analysis. Difference in terms of statistical effect sizes and spatial specificity due to different level of aggregation (voxel- vs. ROI based analysis) were observed but expected.
Randomization	Since the NSPN is an observational desgin, no randomization of subgroups was applicable. We include measures of socioeconomical disadvantage during all analysis as covariate to account for unknown confounding effects of related variable during sampling.
Blinding	Blinding was not relevant to our study since an observational design was used and not an experimental design.

Reporting for specific materials, systems and methods

We require information from authors about some types of materials, experimental systems and methods used in many studies. Here, indicate whether each material, system or method listed is relevant to your study. If you are not sure if a list item applies to your research, read the appropriate section before selecting a response.

Materials & experimental systems

n/a	Involved in the study
☒	☐ Antibodies
☒	☐ Eukaryotic cell lines
☒	☐ Palaeontology
☒	☐ Animals and other organisms
☐	☒ Human research participants
☒	☐ Clinical data

Methods

n/a	Involved in the study
☒	☐ ChIP-seq
☒	☐ Flow cytometry
☐	☒ MRI-based neuroimaging

Human research participants

Policy information about studies involving human research participants

Population characteristics	The NSPN study used an accelerated longitudinal design to investigate psychiatric traits and brain maturation during adolescence and early adulthood. Subjects were sampled in six age bins 14-15y, 16-17y, 18-19y, 20-21y, and 22-24y, with roughly balanced numbers (overall age mean (std) 19.45 (2.85) years). Each age bin was balanced for sex and ethnicity (relative to the local population). From the 2406 participants that took part in the study and which filled out socio-demographic information and questionnaires at least once, 318 healthy subjects (~60 subjects per age bin) participated in the MRI arm (after screening out subjects with self-reported pervasive neurological, developmental or psychiatric disorders). More details can be found in Kiddle, B. et al. Cohort profile: The NSPN 2400 Cohort: a developmental sample supporting the Wellcome Trust NeuroScience in Psychiatry Network. Int. J. Epidemiol. (2017). doi:10.1093/ije/dyx117
Recruitment	Participants were recruited in London and Cambridgeshire from schools, colleges, primary care services and through advertisement. Self-selection bias is likely to operate in at two ways. First, the sample may not be fully representative of the underlying population, in that participants for the scanning study were recruited out of those that returned self-report questionnaires, these were in turn recruited from those that returned and 'expression of interest' form, who were recruited from the target population. Each stage is likely to leave behind more young people who are less planful and/or too stressed and/or too busy to participate in studies. Second, participants were recruited in parallel in the five age bins. The age bins were

balanced with respect to sex and ethnicity, but were not equally easy to fill. Trained research assistants telephoned participants who consented to be contacted and directly asked them to participate in order to fill the age-sex bins that were harder to fill. For example males of age 20 were recuited less readily than females of age 16. Although we do not have direct evidence for this, it could be that ease of recruitment may be correlated with impulsivity, or its neurological correlates, or impulsivity may interact with age to influence recruitment. Such recruitment effects may explain why longitudinal and cross-sectional results may not always concur, so that say young people having their second scan at age 18 differ from the ones recruited to have their first scan at age 18.

Ethics oversight: Ethics were approved by the Cambridge Central Research Ethics Committee (12/EE/0250).

Note that full information on the approval of the study protocol must also be provided in the manuscript.

Magnetic resonance imaging

Experimental design

Design type: accelerated longitudinal observational design

Design specifications: repeated-measures MRI design with 1-3 scans per subject

Behavioral performance measures: To assess self-reported features along obsessive-compulsive and impulsivity spectra, we used well established questionnaires that were handed out to the participants over the course of the study along with baseline MRI acquisitions and follow-ups with up to 3 observations available per person. In particular, we had two measures to assess obsessive-compulsive features, namely the revised Obsessive-Compulsive Inventory (OCI-R) and Padua Inventory (PI-WSUR). For measuring general impulsivity, we used the Barratt Impulsiveness Scale (BIS).

Acquisition

Imaging type(s): multi-echo FLASH Multiparameter Mapping Protocol (longitudinal and transverse relaxation rates R1 and R2*, proton density PD, and magnetization transfer MT) (Weiskopf et al., 2013)

Field strength: 3T

Sequence & imaging parameters: Three different multi-echo FLASH scans were acquired with predominant T1-, PD-, and MT-weighting by appropriate choice of the repetition time (TR) and the flip angle α: TR/α = 18.7 ms/20◦ for the T1w scan and 23.7 ms/6◦ for the PDw and the MTw scans. MT-weighting was achieved by applying an off-resonance Gaussian-shaped RF pulse (4ms duration, 220◦ nominal flip angle, 2 kHz frequency offset from water resonance) prior to the excitation. Multiple gradient echoes were acquired with alternating readout polarity at six equidistant echo times (TE) between 2.2 and 14.7ms for the T1w and MTw acquisi- tions and at 8 equidistant TE between 2.2 ms and 19.7 ms for the PDw acquisition. Other acquisition parameters were: 1 mm isotropic resolution, 176 sagittal partitions, field of view (FOV) = 256 × 240 mm, matrix = 256 × 240 ×176, parallel imaging using GRAPPA factor 2 in phase-encoding (PE) direction, 6/8 partial Fourier in partition direction, non-selective RF excitation, read- out bandwidth BW = 425 Hz/pixel, RF spoiling phase increment = 50◦ , total acquisition time ~19 min. More details can be found in multi-site validation study supporting the reported study. Weiskopf, N., Suckling, J., Williams, G., Correia, M. M., Inkster, B., Tait, R., et al. (2013). Quantitative multi-parameter mapping of R1, PD(*), MT, and R2(*) at 3T: a multi-center validation. Frontiers in Neuroscience, 7, 95. http://doi.org/10.3389/fnins.2013.00095

Area of acquisition: whole-brain MPM acquisition

Diffusion MRI ☐ Used ☒ Not used

Preprocessing

Preprocessing software: MT images were generated based on muli-echo FLASH MPM protocol and hMRI toolbox for SPM (https://github.molgen.mpg.de/VBQ-toolbox-group/hMRI-Toolbox-public). Custom made code based on SPM and CAT toolbox functions is provided along with the manuscript.

First, we performed symmetric diffeomorphic registration.
Second, we applied SPM12's Computational Anatomy Toolbox (CAT, r1318, Structural Imaging Group, http://dbm.neuro.uni-jena.de/cat12/) segmentation to each subject's midpoint image.
Third, nonlinear template generation and image registration to MNI space was performed using the individual midpoint GM and WM tissue maps and diffeomorphic registration using SPM's geodesic shooting .
Fourth, normalized MT maps were smoothed using previously established tissue-weighted-smoothing with a Gaussian kernel of 6 mm full width at half maximum (FWHM) for subcortical and cortical regions, respectively.
Fifth, maps were carefully checked manually before and after longitudinal registration by an expert. Additionally, the obtained normalized and smoothed MT data (in MNI space) was quality checked using statistical covariance-based sample inhomogeneity measures (as implemented in the CAT toolbox) to exclude subjects with extremal overall deviation of quantitative values due to acquisition or processing artefacts.
Finally, we used above within- and between subjects diffeomorphic registration to obtain normalized (gray and white matter) tissue segment maps in the MNI template space for VBM analysis. We accounted for existing differences and ongoing changes of local tissue volumes under applied registrations using both within- and between-subjects modulation. Obtained modulated normalised tissue segments were smoothed using Gaussian filter with 6 mm full width

	at half maximum (FWHM).
Normalization	diffeomorphic registration using geodesic shooting toolbox for SPM (Ashburner & Friston, 2011).
Normalization template	study wise template was generated using geodesic shooting toolbox for SPM
Noise and artifact removal	CAT12 toolbox uses non-local means filtering to reduce local noise levels before segmentation. Since smoothing was applied SNR is improved substantially after accounting for normalization errors. Artifacts were detected manually in terms of visual inspection of movement artifacts and unexpected processing errors were excluded.
Volume censoring	Covariance-based homogeneity checking (CAT toolbox) removing outliers with >2 std in search volume for VBM.

Statistical modeling & inference

Model type and settings	In this study, we performed modelling of the image data using a state-of-the-art analysis method recently introduced as the longitudinal Sandwich Estimator (SwE), http://warwick.ac.uk/tenichols/SwE, SPM toolbox). Using this so-called marginal model one describes individual i's data as $y_i = X_i*\beta + \varepsilon_i*$, i.e. based on only fixed effects design matrix X_i. The randomness is treated as nuisance and modelled by marginal error terms ε_i* with mean 0 and positive semi-definite covariance V_i. Marginal models do not require specification of random-effects and allow unbiased population-average inference and predictions about brain change in certain sub-groups or in relation to covariates.
Effect(s) tested	We tested for positive effects of time/visit, and mean age of individual on MT and according negative effects indicative of shrinkage of volume. We tested for effects of sex and the interactions of those demographic covariates. Moreover we tested for the key hypothesis that higher expression for psychiatric traits were related to impaired growth of MT over visits/time and main effects of traits at baseline.

Specify type of analysis: ☐ Whole brain ☐ ROI-based ☒ Both

Anatomical location(s)	Demographic effects were analyzed on whole-brain voxel-based level since myelination trajectories have not been explored longitudinally before. For trait dimension we focussed a voxel-based analysis on a wholebrain level requested during reviews.
Statistic type for inference (See Eklund et al. 2016)	if not stated otherwise in the manuscript all main findings are based on voxel-wise inference
Correction	FDR, cluster FWE, TFCE

Models & analysis

n/a	Involved in the study
☒	☐ Functional and/or effective connectivity
☒	☐ Graph analysis
☐	☒ Multivariate modeling or predictive analysis

Multivariate modeling and predictive analysis	item-level pca was performed to operationalize the compulsivity dimension